Communication

Reverse Transformation of Deformation-Induced Phases and Associated Changes in the Microstructure of Explosively Clad Ti-5Ta-2Nb and 304L SS

T.N. PRASANTHI, C. SUDHA, S. MURUGESAN, V. THOMAS PAUL, and S. SAROJA

Ti-5Ta-2Nb alloy was joined to 304L austenitic stainless steel by explosive cladding technique. Explosive cladding resulted in the formation of deformation-induced martensite in 304L SS and fcc phase of Ti in the Ti-5Ta-2Nb side of the joint. The stability of these metastable phases was systematically studied using high-temperature X-ray diffraction technique and transmission electron microscopy, which enabled the optimization of the temperature window for post-cladding heat treatments.

DOI: 10.1007/s11661-015-3084-0

The Ti-5Ta-2Nb alloy due to its excellent corrosion resistance and adequate mechanical properties was a candidate structural material for service in concentrated nitric acid environments.[1] 304L austenitic stainless steel (304L SS) with adequate corrosion resistance has been selected for components in non-oxidizing conditions. The development of a sound intermetallic-free joint between Ti-5Ta-2Nb and 304L SS is therefore of high importance for achieving good performance. This dissimilar joint was fabricated using explosive cladding,[2] a solid-state welding technique.

Earlier studies[3–5] revealed that good bond strength could be attained for both similar and dissimilar explosive clads. However, extensive modification in the microstructure of the base materials due to (a) dynamic recrystallization, (b) twinning, and (c) formation of strain-induced phases could not be avoided. Based on detailed investigations on 'as clad' Ti-5Ta-2Nb/304L SS explosive clads,[6,7] the following inferences have been drawn by the authors.

- Explosive clad fabricated with optimized experimental parameters (flyer plate velocity, detonation velocity, stand-off distance, and nature of the explosive) had a wavy interface containing isolated pockets of sub-micron-sized intermetallic phases.
- The clad had adequate bond strength when the tensile axis was parallel to the interface, whereas the bend ductility was inadequate in the perpendicular direction.
- Both 304L SS and Ti-5Ta-2Nb had undergone deformation-induced phase transformation subsequent to explosive cladding.
- The presence of metastable α'(bcc) and ε(hcp) martensite in SS and fcc phase in the Ti alloy,[6] with volume fraction exceeding 0.6, was established by XRD Rietveld analysis.
- Post-cladding, 304L SS exhibited higher tensile and yield strength and reduced ductility, due to formation of martensite, whereas Ti-5Ta-2Nb exhibited a skewed stress–strain curve with no apparent yield point.[8]

The observed degradation in the mechanical property of 304L SS was in agreement with the literature information on biphasic stainless steels.[9] In addition, the presence of strain-induced martensite (SIM) in 300 series SS reduced their resistance to sensitization, pitting corrosion, and hydrogen embrittlement.[10–13] Hence, existence of a biphasic ($\gamma + \alpha'$) structure in the 304L SS side of the explosive clad is undesirable.

The effect of deformation on the corrosion and mechanical properties of multiphase Ti alloys has been studied to a limited extent.[14–16] The presence of fcc phase at the α/β interface inhibits movement of slip, which affects the ductility of the alloys.[14] Polymorphic transformation of hcp to metastable fcc phase has been reported during high-energy ball milling of bulk titanium alloys.[15,16] Based on the calculation of Gibbs energy, Shiyun Xiong *et al.*[17] have proposed that fcc phase was preferred for small (nm range) crystallite sizes of titanium. The stabilization of fcc phase in Ti-5Ta-2Nb can be understood in the light of a possible

T.N. PRASANTHI, Scientific Officer-D, is with the Microscopy and Thermo-Physical Property Division (MTPD), Physical Metallurgy Group (PMG), Metallurgy and Materials Group (MMG), Indira Gandhi Centre for Atomic Research (IGCAR), and also Ph.D. Scholar with the Department of Atomic Energy (DAE), Homi Bhabha National Institute (HBNI), Mumbai, India. C. SUDHA, Scientific Officer-F, is with the Microscopy and Thermo-Physical Property Division (MTPD), Physical Metallurgy Group (PMG), Metallurgy and Materials Group (MMG), Indira Gandhi Centre for Atomic Research (IGCAR). Contact e-mail: sudha_diwa@yahoo.co.in S. MURUGESAN, Scientific Officer-F, and V. THOMAS PAUL, Scientific Officer-E, are with the Materials Synthesis & Structural Characterization Division, Physical Metallurgy Group (PMG), Metallurgy and Materials Group (MMG), Indira Gandhi Centre for Atomic Research (IGCAR). S. SAROJA, Scientific Officer-H+, Head, is with the Microscopy and Thermo-Physical Property Division (MTPD), Physical Metallurgy Group (PMG), Metallurgy and Materials Group (MMG), Indira Gandhi Centre for Atomic Research (IGCAR), and also Professor with the Department of Atomic Energy (DAE), Homi Bhabha National Institute (HBNI).

Manuscript submitted April 23, 2014.
Article published online August 6, 2015

localized deformation, during explosive cladding, resulting in regions of micron- and nano-sized crystallites.[8] The formation of elongated α(hcp) and wedge-shaped fcc grains is a manifestation of the drastic modification of the microstructure due to deformation and expected to influence the corrosion behavior of the alloy.

The present study aims at identification of the temperature and mechanism of the reverse transformation of the metastable phases in 304L SS and Ti alloy to design an appropriate heat treatment to overcome the deterioration in properties for better performance of the clad during service. The thermal stability of metastable phases has been studied by high-temperature X-ray diffraction (HTXRD) technique. The microstructural variations with temperature have been simulated through heat treatments at selected temperatures in the vicinity of the transformation regimes.

Thin specimens of dimension $10 \times 10 \times 2$ mm were extracted from 304L SS and Ti-5Ta-2Nb sides of the clad, very near the interface for the HTXRD analysis. Specimens were polished using standard metallography procedures to obtain flat surfaces. XRD pattern was acquired using INEL XRG-3000 diffractometer (with glancing incidence angle of 5 deg) using Cu Kα radiation. Specimens were heated in a tantalum holder in the temperature range of 373 K to 1373 K (100 °C to 1100 °C) at a heating rate of 20 K (−253 °C)/min. Measurements in the 2θ range from 20 to 90 deg at 2.8×10^{-6} mbar pressure were carried out using a Buhler HDK 2.4 high-temperature camera. Volume fraction (V_f) of metastable phases was calculated from the HTXRD pattern using the following equation[18]:

$$V_f = \frac{\frac{1}{n}\sum_{j=1}^{n} I_A^j / R_A^j}{\frac{1}{n}\sum_{j=1}^{n} I_B^j / R_B^j + \frac{1}{n}\sum_{j=1}^{n} I_A^j / R_A^j}, \quad [1]$$

where 'n' indicates number of peaks of the phase for which volume fraction is to be estimated, 'I' is the integrated intensity, and 'R' is the material scattering factor for the corresponding reflecting plane. Based on the change in V_f with temperature, phase transformation regimes were identified. The microstructures corresponding to these temperatures were generated by heat treatment of the specimen for duration of 2 hours at the selected temperatures and furnace cooled.

Microstructural characterization of the heat-treated specimen was carried out using scanning electron microscope XL30 ESEM of M/s FEI. Leitz microhardness tester with an applied load of 100 g was used for microhardness measurements. Electron transparent thin foils were prepared from 304L SS and Ti-5Ta-2Nb by mechanical polishing followed by jet thinning using a solution of $HClO_4$(10 pct) + CH_3OH(90 pct). Bright-field (BF) images and selected area diffraction (SAD) patterns were obtained from these thin foils using PHILIPS CM200 transmission electron microscope (TEM) at an operating voltage of 200 kV.

Figures 1(a) and (b) show the room-temperature XRD patterns of the two parent materials 304L SS and Ti-5Ta-2Nb, respectively, used for fabrication of explosive clads, revealing the Bragg diffraction peaks corresponding to fcc(γ) phase in 304L SS and the α(hcp) + β(bcc) phases in Ti-5Ta-2Nb alloy.[6] Figures 2(a) and (b) show the typical TEM BF image and the corresponding SAD pattern obtained from the SS side of the 'as clad.' Figure 2(a) shows the presence of martensite laths. Analysis of the SAD pattern (Figure 2(b)) obtained from the intersection of martensite laths provides evidence for the presence of α-Fe (bcc) phase along [$\bar{1}$11] zone axis. The formation of α′ has been rationalized based on strain rates higher than shock loading conditions in 304L SS base plate during explosive cladding. The α′ nucleation sites along shear bands, shear band intersections, and twin boundaries and the presence of ε martensite have been reported in detail in TEM studies.[7]

Figure 3(a) shows a representative TEM-BF image from 'as clad' Ti-5Ta-2Nb showing elongated grains of

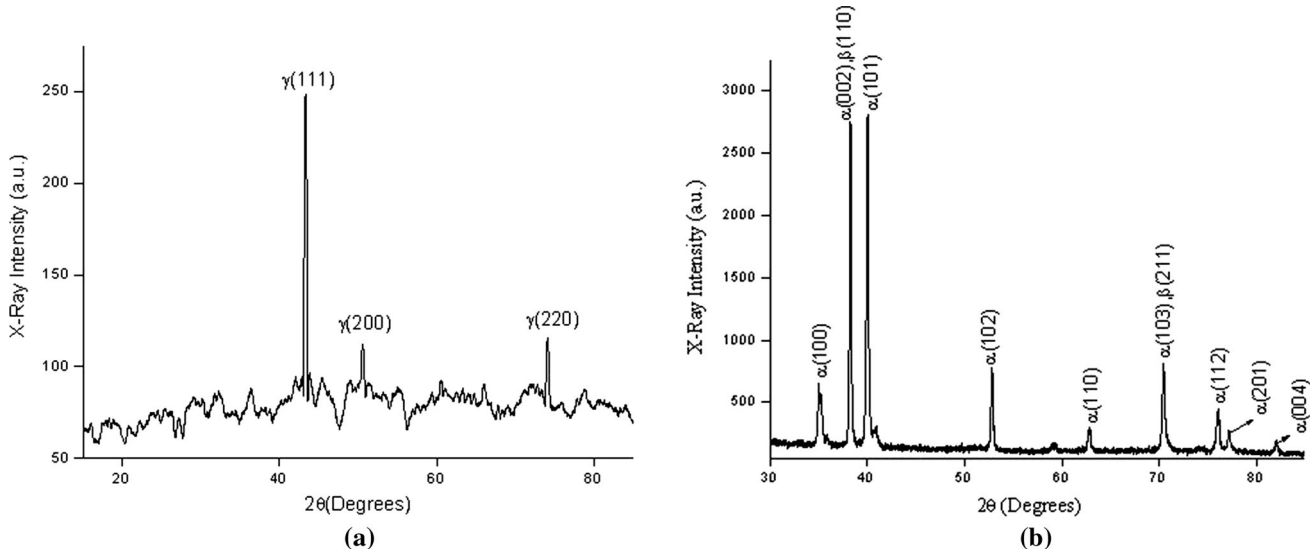

Fig. 1—XRD pattern obtained from (*a*) 304L SS and (*b*) Ti-5Ta-2Nb before explosive cladding process.

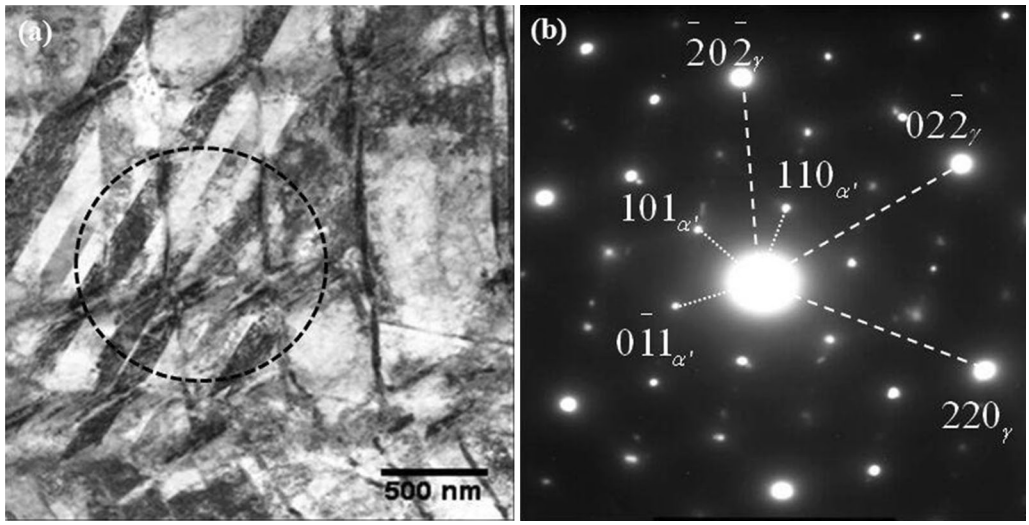

Fig. 2—(*a*) TEM-BF image showing martensite laths, (*b*) SAD pattern (obtained from the circled region in (a)) confirms presence of α' and γ phases along $[\bar{1}11]$ and $[\bar{1}11]$ zone axis, respectively.

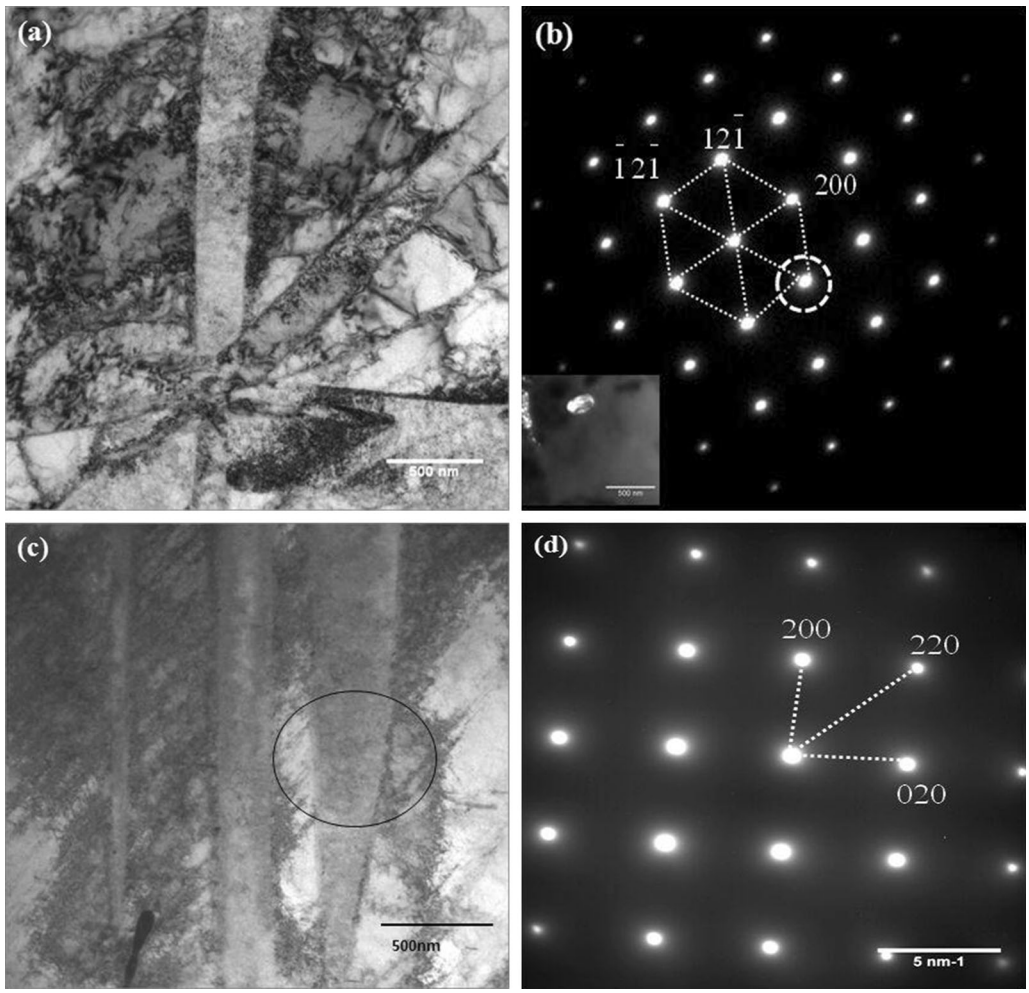

Fig. 3—(*a*) TEM-BF image obtained from 'as clad' Ti-5Ta-2Nb showing elongated α grains of Ti, (*b*) SAD pattern confirming the presence of β phase along [012] zone axis; inset is the dark-field image corresponding to the circled diffraction spot revealing globular β particles along $[1\bar{2}1]$ orientation, (*c*) TEM-BF image showing regions with unique wedge-shaped morphology, and (*d*) SAD pattern along [001] zone axis obtained from the circled region in (c) confirming the presence of fcc phase of Ti.

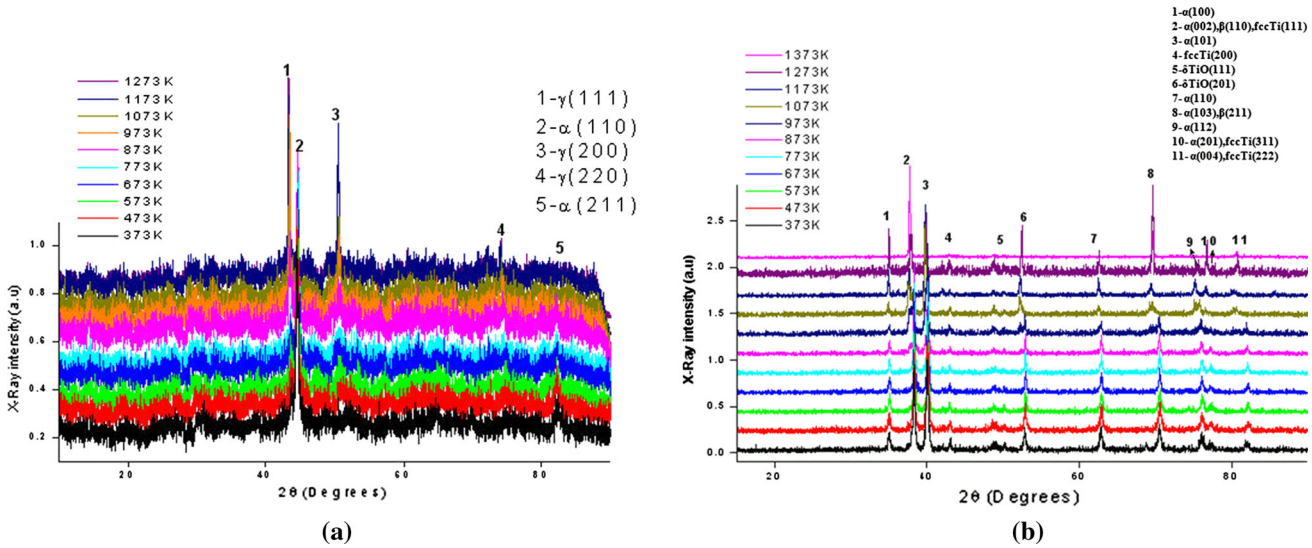

Fig. 4—HTXRD patterns obtained from 'as clad' (*a*) 304L SS and (*b*) Ti-5Ta-2Nb alloy, respectively.

α. Globular precipitates of 150 to 200 nm diameter were also present along the α grain boundaries. Figure 3(b) shows the SAD pattern obtained from one such globular particle identified as β phase along [012] zone axis. The inset shows the dark-field image corresponding to the circled diffraction spot in the SAD pattern further confirming the presence of β phase. Figure 3(c) shows the BF image from the same specimen revealing a region with unique wedge-shaped morphology. Analysis of the corresponding electron diffraction pattern (Figure 3(d)) identified these regions as fcc Ti phase. The 'as clad' Ti-5Ta-2Nb structure can therefore be summarized as $\alpha(\text{hcp}) + \beta(\text{bcc}) + \gamma(\text{fcc})$.

Figures 4(a) and (b) show the HTXRD patterns in the temperature range of 373 K to 1373 K (100 °C to 1100 °C) obtained from the deformed 304L SS and Ti-5Ta-2Nb alloy, respectively. Figure 4(a) shows strong Bragg reflections corresponding to the α′ phase at 373 K (100 °C), the lowest temperature of exposure. No significant change occurred in the X-ray intensity of α′ until 773 K (500 °C), beyond which it decreased until 1073 K (800 °C), and only γ phase was observed between 1073 K and 1373 K (800 °C and 1100 °C). The volume fraction $V_f(\alpha')$ was estimated using Eq. [1] based on intensity ratios, and Figure 5 shows the calculated $V_f(\alpha')$ plotted as a function of temperature. $V_f(\alpha')$ remained constant (~0.63) until 773 K (500 °C) and gradually reduced to ~0.16 at 1073 K (800 °C). Beyond 1073 K (800 °C), α′ peaks could not be clearly distinguished. Based on the observed variation of $V_f(\alpha')$, four temperatures in the range of 673 K to 973 K (400 °C to 700 °C) were selected for further heat treatment of 304L SS using thin specimens extracted from the clad.

Figure 4(b) shows the predominance of Bragg reflections corresponding to α and fcc phases of Ti until 1073 K (800 °C), while individual reflections of β phase could not be detected due to its low volume fraction. Although the highest intensity peak for the fcc phase

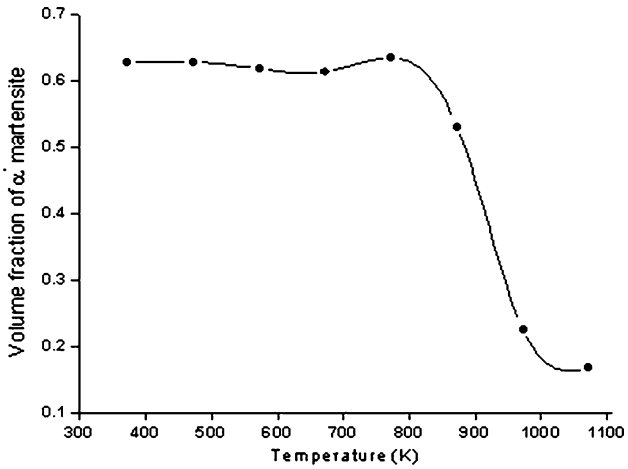

Fig. 5—Change in the volume fraction of α′ phase in 'as clad' 304L SS with heat treatment.

overlapped with (002)α, its presence was unambiguously confirmed from the additional (200) peak. A peak corresponding to TiO was observed at all temperatures due to the oxidation of titanium during the experiment. A rigorous comparison was made for the experimentally observed reflections in Figure 4(b) against all possible reflections of various Ti phases and compounds mainly oxides and nitrides of Ti, Ta, and Nb to avoid any erroneous identification. Beyond 1073 K (800 °C), β phase was dominant due to the allotropic transformation of titanium. Volume fraction of fcc phase although semi-quantitative was calculated from the intensity ratios in XRD patterns to know the trend as explained earlier. Figure 6 shows the variation in the volume fraction of fcc phase with temperature. The volume fraction showed a systematic decrease with ~0.48 at the lowest temperature of 373 K (100 °C), which reduced to ~0.23 only beyond 873 K (600 °C).

The microstructural changes in 304L SS and Ti-Ta-Nb associated with the variation in the volume fraction of metastable phases, obtained by simulated heat treatments, are described in sequence in subsequent sections. Figure 7 highlights the changes in the microstructure of 304L SS in 'as clad' condition and as a function of temperature [673 K, 873 K, and 973 K (400 °C, 600 °C, and 700 °C)] along with the corresponding hardness values. Figure 7(a) shows the deformed structure with a high value of hardness of ~375 VHN in 'as clad' condition. Deformed grains were observed up to the temperature of 873 K (600 °C) (Figures 7(b) and (c)), while more equiaxed grains were observed at 973 K (700 °C) which is also reflected in the reduced value of hardness of ~271 VHN (Figure 7(d)). It is important to note that the hardness is still higher than that of parent material (~230 VHN), which provides evidence for the retention of α' phase at 873 K (600 °C).

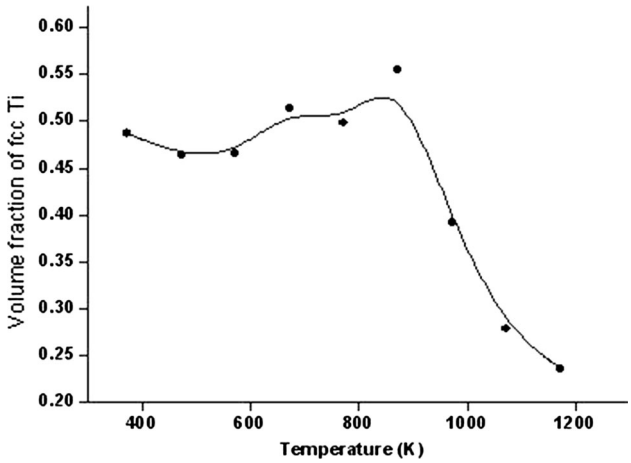

Fig. 6—Change in the volume fraction of metastable fcc phase in 'as clad' Ti-5Ta-2Nb alloy with heat treatment.

HTXRD-based investigations revealed that thermal exposure of biphasic 304L SS beyond 873 K (600 °C) will result in significant reversion of SIM to parent γ phase. This observation agreed with the reported temperature window [673 K to 1073 K (400 °C to 800 °C)] for $\alpha' \rightarrow \gamma$ reverse transformation in 304L SS.[19] In literature,[20] two mechanisms have been suggested for $\alpha' \rightarrow \gamma$ reverse transformation: (1) athermal shear and (2) isothermal diffusion. Shear reversed γ will be associated with high density of dislocations and diffusion-induced γ will nucleate on prior existing deformed γ grains and martensite phase. Both these mechanisms are probable in 304L SS having low stacking fault energy. Further electron-microscopy-based investigations are in progress to confirm the exact reverse transformation mechanism in explosively clad and heat-treated SS.

Figures 8(a) through (d) are the SE images obtained from Ti-5Ta-2Nb in 'as clad' condition and after heat treatment at 373 K, 873 K, and 1173 K (100 °C, 600 °C, 900 °C), respectively. In the 'as clad' condition (Figure 8(a)), the elongation of grains in the direction of propagation of the explosive waves is evident. Figure 8(b) shows the retention of deformed grains at

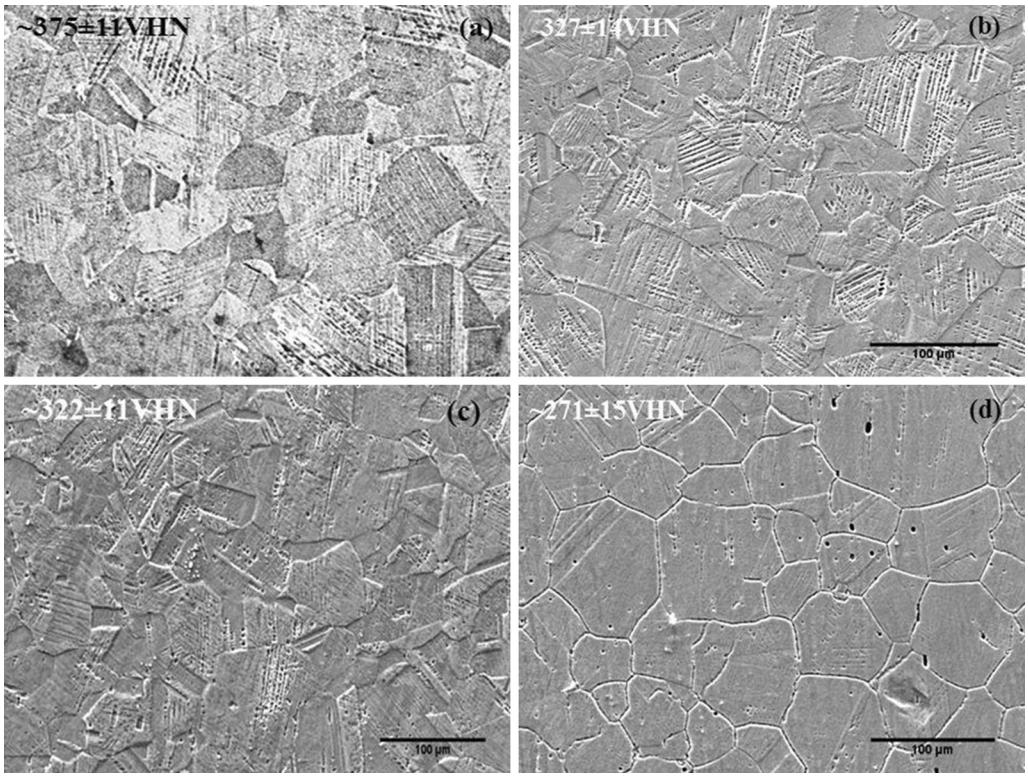

Fig. 7—Secondary electron (SE) image of 304L SS (*a*) in 'as clad' condition and indicating change in the microstructure after heat treatment at (*b*) 673 K (400 °C), (*c*) 873 K (600 °C), and (*d*) 973 K (700 °C), respectively.

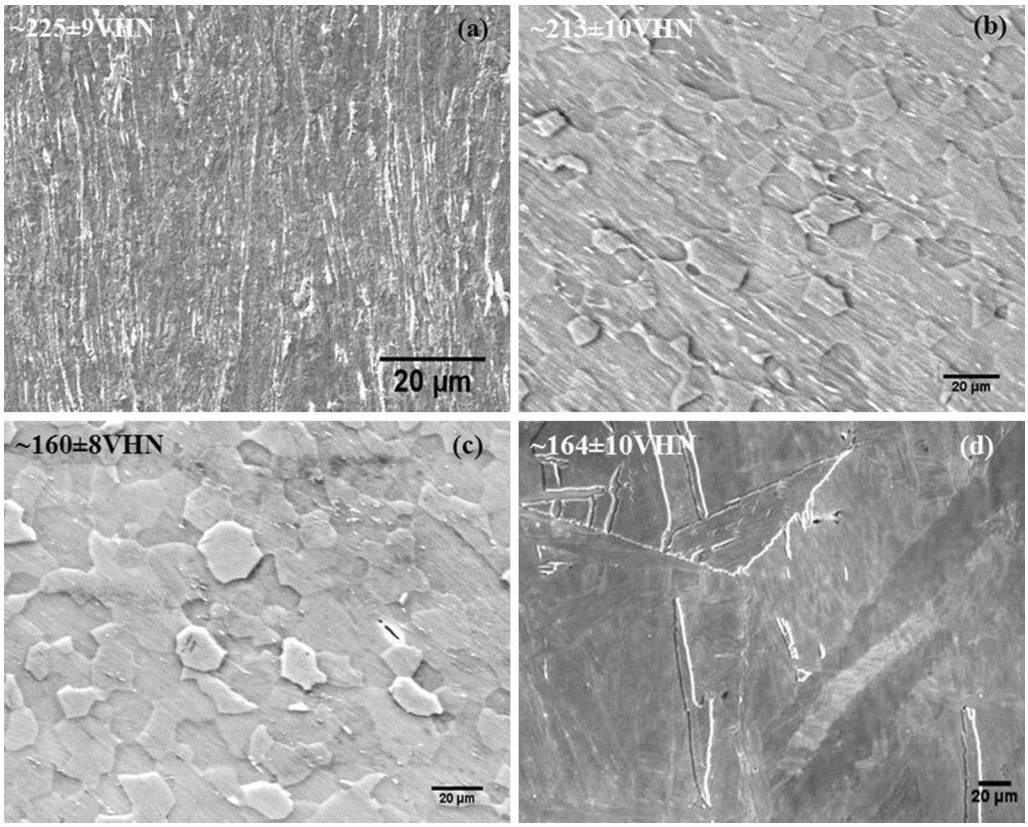

Fig. 8—SE micrograph of Ti-5Ta-2Nb (*a*) in 'as clad' condition and showing change in the microstructure after heat treatment at (*b*) 373 K (100 °C), (*c*) 873 K (600 °C), and (*d*) 1173 K (900 °C), respectively.

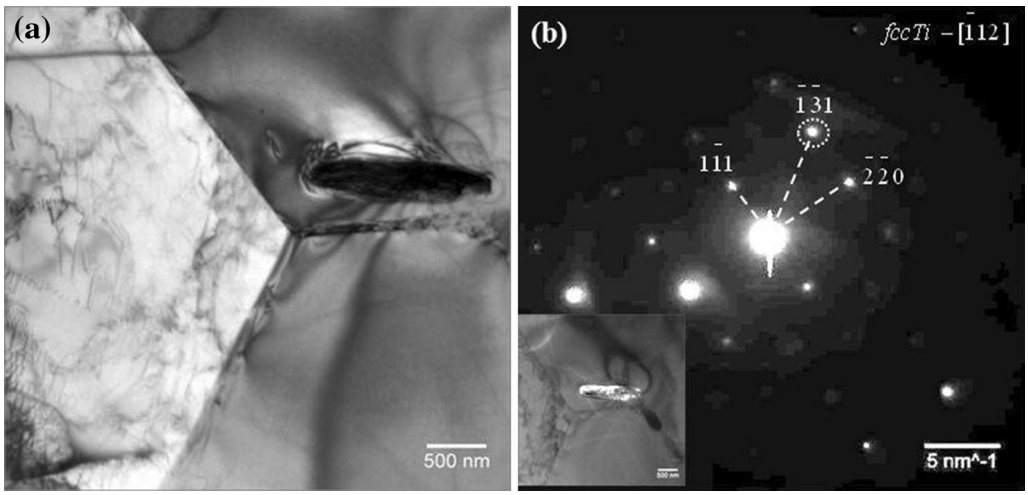

Fig. 9—(*a*) TEM-BF image obtained from 'as clad' Ti-5Ta-2Nb after heat treatment at 873 K (600 °C) for 2 h showing an acicular particle and (*b*) Corresponding SAD pattern along $[\bar{1}12]$ zone axis confirming it to be the fcc phase; inset is the dark-field image for $[\bar{1}\bar{3}1]$ orientation of the fcc phase.

373 K (100 °C), and nucleation of α grains from the deformed structure is seen from Figure 8(c). A martensite structure within large prior β grains indicates extensive grain growth at high temperatures, the subsequent transformation of the β to martensite at 1173 K (900 °C) (Figure 8(d)). The hardness shows an expected trend, reaching a value corresponding to the parent alloy beyond 873 K (600 °C).

To get confirmatory evidence for the presence of low volume fraction of fcc phase near the transformation regime, thin foil specimen of Ti-5Ta-2Nb heat treated at a temperature of 873 K (600 °C) was examined using TEM. Figure 9(a) is the BF image that shows equiaxed grains in addition to a region exhibiting acicular morphology. Analysis of the SAD pattern (Figure 9(b)) obtained from this region confirmed it to have fcc

crystal structure along $[\bar{1}12]$ zone axis. Dark-field image (inset in Figure 9(b)) corresponding to the circled spot in Figure 9(b) further confirmed the acicular region to be the fcc phase present along $[\bar{1}\bar{3}1]$ orientation. Compared to 'as clad' Ti-5Ta-2Nb (Figure 3(c)), regions exhibiting fcc structure were much finer (≤1 μm).

Similar to the observation made in SS side of the clad, heat treatment at temperatures beyond 873 K (600 °C) was sufficient to drastically reduce the volume fraction of metastable phase in Ti-5Ta-2Nb. To the best of our knowledge, there is no information available in the literature on the reverse transformation mechanism of fcc to α-Ti phase. Further investigations are in progress to identify this which is beyond the scope of this work.

For industrial applications, 'as clad' plates are generally heat treated to remove residual stresses and improve ductility. Present investigation on the stability of deformation-induced phases in the base materials of the clad revealed that it is necessary to expose the explosive clad to temperatures >873 K (600 °C). This will help in minimizing the effect of metastable phases on mechanical and corrosion properties of the clad especially with respect to martensite in SS. However, it is essential to optimize the temperature–time window in concurrence with the knowledge on evolution of interface microstructure due to inter-diffusion of alloying elements across the clad interface.

The authors thank Dr. P.R. Vasudeva Rao, Director, IGCAR, Dr. T. Jayakumar, former Director, Metallurgy and Materials Group, and Dr. M. Vijayalakshmi, Associate Director, Physical Metallurgy Group, IGCAR for their encouragement and support throughout the period of this work.

REFERENCES

1. B. Raj and U. Kamachi Mudali: *Prog. Nucl. Energy*, 2006, vol. 48, pp. 283–313.
2. R.V. Tamhankar and J. Ramesam: *Mater. Sci. Eng.*, 1974, vol. 13, pp. 245–54.
3. F. Findik: *Mater. Des.*, 2011, vol. 32, pp. 1081–93.
4. H.B. Xia, S. Wang, and H. Ben: *Mater. Des.*, 2014, vol. 56, pp. 1014–19.
5. B. Wronka: *J. Mater. Sci.*, 2010, vol. 45, pp. 4078–83.
6. C. Sudha, T.N. Prasanthi, S. Murugesan, S. Saroja, P. Kuppusami, and M. Vijayalakshmi: *Sci. Technol. Weld. Join.*, 2011, vol. 16, pp. 133–39.
7. C. Sudha, T.N. Prasanthi, V. Thomas Paul, S. Saroja, and M. Vijayalaksmi: *Metall. Mater. Trans.*, 2012, vol. 43A, pp. 3596–3607.
8. C. Sudha, T.N. Prashanti, V. Thomas Paul, S. Saroja, and M. Vijayalakshmi: *Procedia Eng.*, 2014, vol. 86, pp. 42–50.
9. A. Das, S. Tarafder, and P.C. Chakraborti: *Mater. Sci. Eng. A*, 2011, vol. 529, pp. 9–20.
10. M. Smaga, F. Walther, and D. Eifler: *Mater. Sci. Eng. A*, 2008, vols. 483–84, pp. 394–97.
11. W. Ozgowicz, A. Kurc, and M. Kuick: *Arch. Mater. Sci. Eng.*, 2010, vol. 43, pp. 42–53.
12. M. Stalder, S. Vogel, M.A.M. Bourke, J.G. Maldonado, D.J. Thoma, and V.W. Yuan: *Mater. Sci. Eng. A*, 2000, vol. 280, pp. 270–81.
13. M. Martin, S. Weber, C. Izawa, S. Wagner, A. Pundt, and W. Theisen: *Int. J. Hydrog. Energy*, 2011, vol. 36, pp. 11195–1206.
14. F. Li, J. Mo, J. Li, J. Huang, W. Fan, and J. Fang: *Procedia Eng.*, 2014, vol. 81, pp. 754–59.
15. I. Manna, P.P. Chattopadhyay, P. Nandi, F. Banhart, and H.J. Fecht: *J. Appl. Phys.*, 2003, vol. 93 (3), pp. 1520–24.
16. A.J. Phasha, H. Kasonde, and P.E. Ngoepe: 2008. http://researchspace.csir.co.za/dspace/bitstream/…/1/Phasha_P_2008.pdf.
17. S. Xiong, W. Qi, B. Huang, M. Wang, and Y. Li: *Mater. Chem. Phys.*, 2010, vol. 120, pp. 446–51.
18. L.V. Jinlong and L. Hongyun: *Mater. Sci. Eng. C*, 2014, vol. 34, pp. 484–90.
19. I. Meszaros and J. Prohaszka: *J. Mater. Process. Technol.*, 2005, vol. 161, pp. 162–68.
20. A. Rezaee, A. Najafizadeh, A. Kermanpur, and M. Moallemi: *Mater. Des.*, 2011, vol. 32, pp. 4437–42.